99mTc-MIBI SPECT in Distinguishing Neoplastic from Nonneoplastic Intracerebral Hematoma

Fabio Minutoli, MD[1]; Filippo F. Angileri, MD[2]; Sebastiano Cosentino, MD[1]; Giorgio Restifo Pecorella, MD[1]; Salvatore Cardali, MD[2]; Oreste De Divitiis, MD[2]; Antonino Germanò, MD[2]; and Sergio Baldari, MD[1]

[1]Department of Radiological Sciences, University of Messina, Messina, Italy; and [2]Department of Neurosurgery, University of Messina, Messina, Italy

Distinguishing neoplastic from nonneoplastic intracerebral hematoma has great clinical relevance for the appropriate management of patients. Imaging is not always able to clearly identify a tumor-related intraparenchymal cerebral hemorrhage (ICH), especially in the acute phase, the diagnosis being frequently based on evolution patterns. The aim of this study was to test the value of 99mTc-methoxyisobutylisonitrile (99mTc-MIBI) SPECT as a noninvasive diagnostic tool in early diagnosis of hemorrhagic brain neoplasm. **Methods:** We prospectively studied 29 patients harboring a nontraumatic acute onset of clinical deterioration caused by ICH with atypical clinical or neuroradiologic features. All patients underwent 99mTc-MIBI SPECT within 48 h from the clinical onset. Early and delayed images were obtained. Both visual and semiquantitative analyses were performed. The 99mTc-MIBI index was obtained from both early and delayed images and the retention index was calculated. **Results:** In 19 patients (65.5%), a nonneoplastic hemorrhage (15 vascular degenerative diseases, 2 cavernous angiomas, 1 thrombosed middle cerebral artery giant aneurysm, and 1 sinus rectus thrombosis) was diagnosed by clinical and neuroradiologic follow-up or open surgery. In 10 patients (34.5%), a neoplastic hemorrhage (6 metastases, 2 glioblastomas multiforme, 1 ependymoma, and 1 intracranial angioblastic meningioma) was diagnosed by direct histologic typing (open surgery or stereotactic biopsy). In all neoplasm-related hemorrhages, a focal increased tracer uptake was observed in the area of the lesion, whereas no focal increased tracer uptake was noted in all nonneoplastic hematomas. A wide cutoff in the early ratio between neoplastic and nonneoplastic hemorrhages was found. Moreover, a statistically significant difference was found in the delayed ratio ($P < 0.01$) and the retention index ($P < 0.05$) between the 2 groups. **Conclusion:** Our data suggest that 99mTc-MIBI SPECT could play a role in the early noninvasive diagnostic work-up of hemorrhagic brain lesions, allowing a clear differentiation between neoplastic and nonneoplastic ICHs. The high availability and low cost of this nuclear medicine technique can be considered additional advantages.

Key Words: 99mTc-methoxyisobutylisonitrile; SPECT; brain tumor; intracranial hemorrhage

J Nucl Med 2003; 44:1566–1573

Distinguishing neoplastic from nonneoplastic intracerebral hematoma represents a significant challenge for clinicians and researches, since neoplasms can be hidden behind an intraparenchymal cerebral hemorrhage (ICH) (*1–6*) and some hemorrhagic nonneoplastic lesions may mimic neoplasms on standard neuroradiologic images (*7–12*). This differential diagnosis, especially in the acute phase, has significant clinical relevance for the appropriate management of patients.

Although some studies have been specifically addressed the neuroradiologic and nuclear medicine features to diagnose neoplasm-related ICH, a confident diagnosis is impossible in many cases. Moreover, the differential diagnosis between neoplastic and nonneoplastic ICH is frequently based on evolution patterns, often delaying the appropriate management of patients (*13–22*).

99mTc-Methoxyisobutylisonitrile (99mTc-MIBI) has been used as an imaging SPECT agent for various neoplasms, including brain tumors. High-grade astrocytomas, glioblastomas multiforme, metastases, intracranial meningiomas, and neurinomas show high 99mTc-MIBI uptake. On the other hand, nonneoplastic lesions show no or low 99mTc-MIBI accumulation (*23–33*). Thus, there are hypothetic grounds to approach the differentiation between neoplastic and nonneoplastic ICH by means of 99mTc-MIBI SPECT.

The aim of this study was to test the value of 99mTc-MIBI SPECT as a noninvasive diagnostic tool in early diagnosis of hemorrhagic brain neoplasms.

MATERIALS AND METHODS

Patient Population

Between March 1999 and September 2001, in our Department of Neurosurgery, we prospectively studied 29 patients (14 men, 15 women; mean age, 55 y; range, 27–80 y) harboring an acute onset of clinical deterioration caused by ICH.

Each patient had to meet all of the following inclusion criteria: (a) nontraumatic acute onset of neurologic deterioration occurred; (b) ICH was demonstrated by emergency CT scan; (c) clinical data (young age, negative medical history for arterial hypertension, diabetes, drug abuse, and anticoagulant or antiplatelet medication therapy) or findings on emergency CT scan (atypical location, irregular shape, disproportional large edema) could be compatible
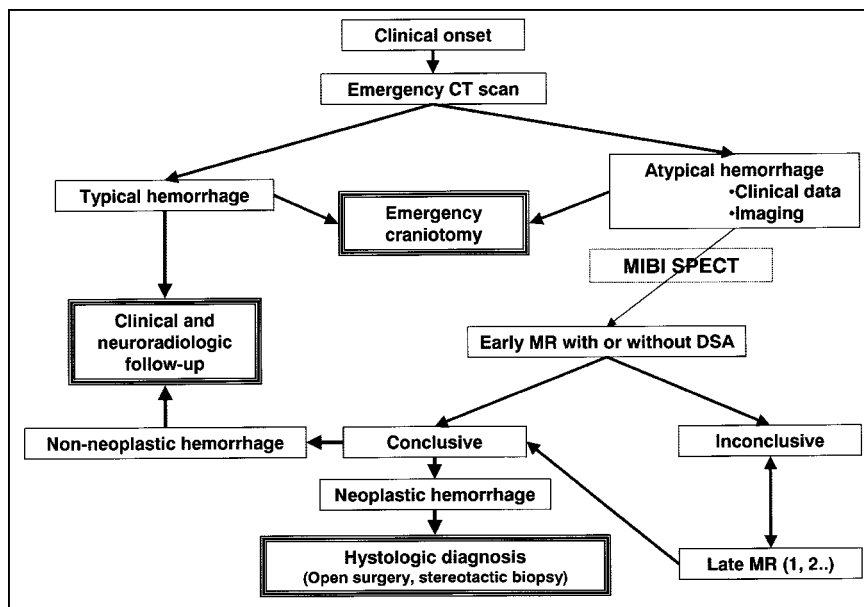
FIGURE 1. Flow chart describing diagnostic work-up for patients harboring nontraumatic intracerebral hemorrhage at our institution. DSA = digital subtraction angiography.

with a neoplastic hemorrhage; (d) the patient did not have any known brain neoplasm; (e) a single lesion was evident on brain CT scan; and (f) emergent craniotomy was not required. In this series, we excluded those cases with pituitary, pure subarachnoid, and pure intraventricular hemorrhage.

After acquiring an emergency-admission CT scan, all patients in this study underwent ^{99m}Tc-MIBI SPECT within 48 h from the clinical onset. Apart from ^{99m}Tc-MIBI SPECT findings (neurosurgeons and neuroradiologists were unaware of the ^{99m}Tc-MIBI SPECT results), patients underwent a neuroradiologic protocol constituted by an early standard MR examination and ≥1 additional MR examinations if required by nondefinitive diagnosis. If MR examination could not be performed, ≥1 contrast-enhanced CT scans were obtained. Moreover, some patients underwent digital subtraction angiography at a different time if needed (Fig. 1). Patients were followed-up until a definitive diagnosis was obtained.

The study was approved by our institutional review board, and informed consent was obtained from each patient.

^{99m}Tc-MIBI SPECT Protocol

Images were acquired on a dual-head gamma camera (Odissey; Picker International), using a circular orbit and high-resolution collimators with a 128 × 128 matrix, 360° rotation, a 3° step-and-shoot technique, and an acquisition time of 25 s per frame, 10 min (early images) and 3 h (delayed images) after intravenous injection of 740 MBq (20 mCi) ^{99m}Tc-MIBI. The data were processed, after a ramp-filtered backprojection and an attenuation correction (correction factor, 0.110), using a low-pass filter. The data were displayed 2-pixels thick (4.6 mm) in the transaxial, sagittal, and coronal slices, followed by orbitomeatal line reorientation of the reconstructed volume.

SPECT Data Analysis

^{99m}Tc-MIBI SPECT studies were visually and semiquantitatively evaluated by 2 independent nuclear medicine physicians (1 experienced and 1 less experienced) with the knowledge of the emergency CT results.

The visual analysis was conducted as follows: A study was considered consistent with nonneoplastic ICH when absent or faint increased activity was seen and consistent with neoplastic ICH when there was clear increased tracer uptake compared with that of the contralateral side.

For the semiquantitative analysis, after spatial localization of the lesion, using CT as a guide, a round-shaped region of interest (ROI) was drawn encompassing the maximum uptake area in the region of the lesion. During this procedure, images were displayed with base and window setting held constant. The ^{99m}Tc-MIBI index was obtained as the ratio of counts in the lesion ROI to the counts in its contralateral homologous mirror image. If the control ROI was close to the scalp or the choroid plexus or a midline-located lesion was revealed, the control ROI was drawn on an uninvolved cerebral parenchymal area. The ^{99m}Tc-MIBI index was obtained from both early images (early ratio) (ER) and delayed images (delayed ratio) (DR). In addition, a retention index ([RI]; i.e., ratio between DR and ER) was calculated.

Statistical Analysis

Statistical analysis was made on the basis of data provided by the first observer. Definitive diagnoses were used as the standard of reference. In addition, data determined by the 2 observers were matched for interobserver variability evaluation.

Values of sensitivity, specificity, accuracy, and positive and negative predictive values in revealing neoplasm-related ICH were calculated for visual analysis.

The Student t test for unpaired data was used to calculate a 2-sided P value when comparing the ER, DR, and RI for the 2 groups. Differences were considered significant when $P < 0.05$.

Interobserver variability was measured using the κ-statistic.

RESULTS

In 19 patients (65.5%), a nonneoplastic hemorrhage (15 vascular degenerative diseases, 2 cavernous angiomas, 1 thrombosed middle cerebral artery giant aneurysm, and 1 sinus rectus thrombosis) was diagnosed (Fig. 2). In 15 of 19
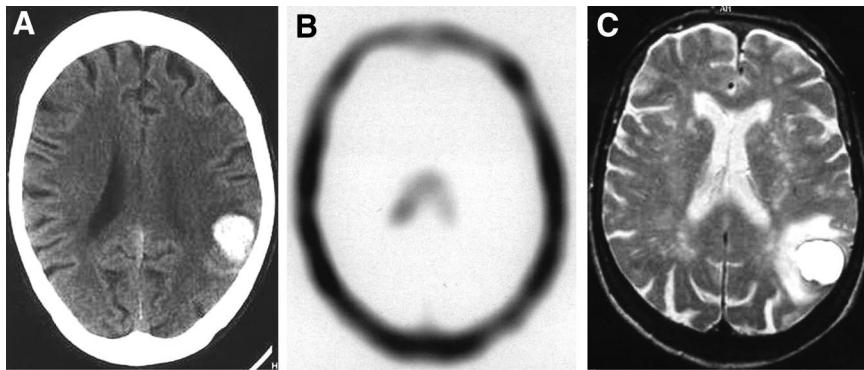
FIGURE 2. Patient 21: 76-y-old woman with sudden onset of cephalea and aphasia. Medical history did not reveal any significant findings. (A) Emergency CT scan shows atypically located 25-mm large round-shaped cortical hematoma in left parietal region. Lesion is surrounded by moderate edema. (B) Early ^{99m}Tc-MIBI SPECT image shows no focal ^{99m}Tc-MIBI uptake areas (ER = 1.04). (C) T2-weighted spin-echo MR image obtained 13 d after clinical onset shows lesion as homogeneous hyperintense core with peripheral thin hypointense rim surrounded by moderate edema. Mass effect is minimal. These features suggested vascular degenerative disease. One-year follow-up supports this diagnosis.

patients, the diagnosis was reached on the basis of clinical and neuroradiologic follow-up. In 4 of 19 patients, diagnosis was reached by means of open surgery. In 1 patient, hematoma evacuation was needed because of delayed deterioration due to increasing mass effect that was not responsive to medical therapy. In 2 patients with MRI findings of cavernous angioma, definitive diagnosis was reached after surgical excision. In another patient, on the basis of early MRI findings, a tumor-related hemorrhage was suspected but surgery revealed a thrombosed middle cerebral artery giant aneurysm (Fig. 3).

In 10 patients (34.5%), a neoplastic hemorrhage (6 metastases, 2 glioblastomas multiforme, 1 ependymoma, and 1 intracranial angioblastic meningioma) was diagnosed by direct histologic typing (open surgery or stereotactic biopsy) (Figs. 4 and 5). In 2 patients of this group, MRI was contraindicated, because of the presence of a cardiac pacemaker, and contrast-enhanced CT was obtained.

In 2 of 6 metastatic patients, a primary neoplasm was unknown at admission.

Visual analysis showed no focal increased tracer uptake in all nonneoplastic hemorrhages, whereas it showed a focal increased tracer uptake in all neoplastic lesions (Table 1). Sensitivity, specificity, accuracy, and positive and negative predictive values in revealing neoplasm-related ICH by means of ^{99m}Tc-MIBI SPECT were 100%.

For the semiquantitative analysis, in nonneoplastic hemorrhages, the ER ranged between 0.89 and 1.3 (mean, 1.03 ± 0.1), the DR ranged between 0.9 and 1.18 (mean, 1.01 ± 0.06), and the RI ranged between 0.77 and 1.07 (mean, 0.98 ± 0.08). In neoplastic hemorrhages, the ER ranged between 2 and 5.5 (mean, 2.96 ± 1.14), the DR ranged between 1 and 3.3 (mean, 2.07 ± 0.71), and the RI ranged between 0.38 and 1.03 (mean, 0.74 ± 0.25) (Table 1). A wide cutoff in the ER between neoplastic hemorrhages and nonneoplastic hemorrhages was found (Fig. 6). Moreover, a statistically significant difference
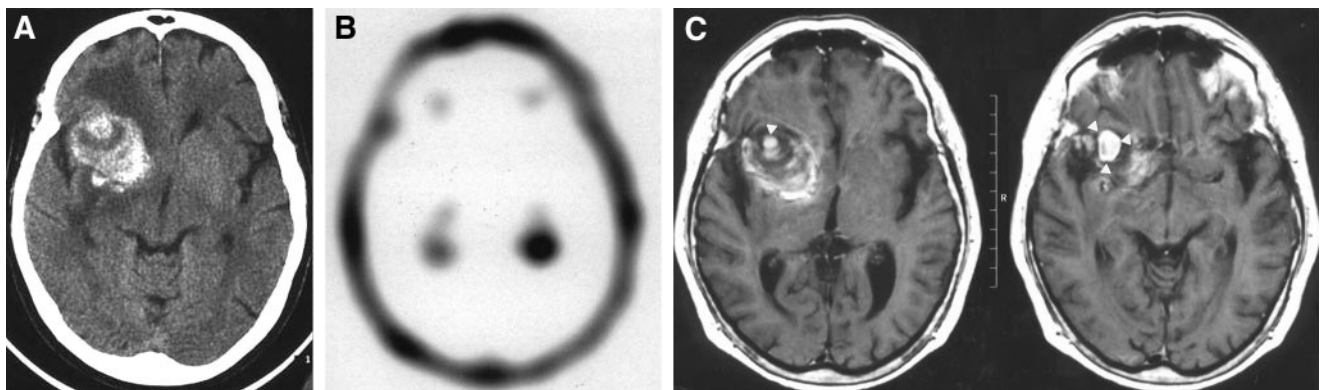
FIGURE 3. Patient 27: 52-y-old woman with sudden onset of stupor and mild left hemiparesis. Medical history did not reveal any significant findings. (A) Emergency CT scan reveals 4.5-cm large insular nonhomogeneously hyperdense mass surrounded by discrete edema with significant mass effect. (B) Early ^{99m}Tc-MIBI SPECT image shows no focal areas of high ^{99m}Tc-MIBI accumulation in area of lesion (ER = 1.3). (C) T1-weighted MR images after intravenous gadolinium administration show nonhomogeneous hemorrhagic lesion with small enhancing area (arrowheads). Digital subtraction angiography (not shown) failed to reveal relevant data. Patient underwent surgery and right thrombosed giant middle cerebral artery aneurysm was found.
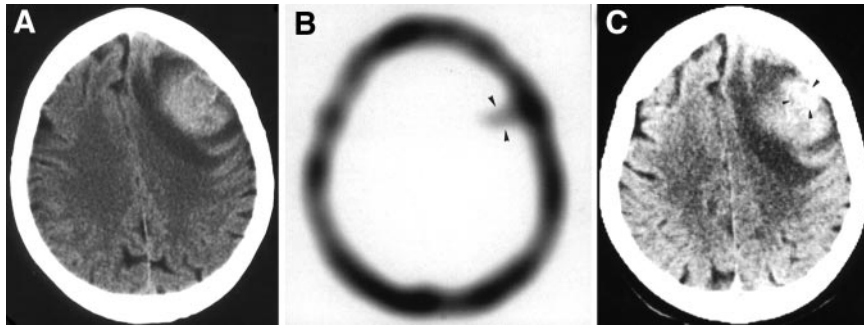
FIGURE 4. Patient 2: 72-y-old woman with sudden onset of aphasia and right-sided severe hemiparesis. Medical history revealed arterial hypertension. (A) Emergency CT scan reveals 4-cm large left frontal lobe oval-shaped hyperdense mass with surrounding edema and discrete mass effect. (B) Early ^{99m}Tc-MIBI SPECT image shows focal high ^{99m}Tc-MIBI uptake in area of lesion (ER = 2.13) (arrowheads). (C) After contrast medium administration, CT shows 15-mm round-shaped nodule with homogeneous contrast enhancement (arrowheads). After stereotactic biopsy, metastasis from cutaneous melanoma was demonstrated.

was found in the DR ($P < 0.01$) and the RI ($P < 0.05$) between the 2 groups (Fig. 7).

No significant statistical differences were found in the ER, DR, and RI between vascular degenerative diseases and other etiologies (cavernous malformations, aneurysm, and dural sinus thrombosis) in the nonneoplastic group (all $P > 0.5$).

Finally, there was complete agreement between the 2 observers for visual analysis and interobserver agreement was excellent for the ER ($\kappa = 0.98$), DR ($\kappa = 0.95$), and RI ($\kappa = 0.95$).

DISCUSSION

The radiologic finding of cerebral hematoma does not represent a diagnosis; rather, hemorrhage should always be presumed to be the result of a primary disease or degenerative condition, whose correct identification usually has important implications in developing a treatment plan (*34*).

During daily clinical practice, it is important to remember that sometimes neoplasms can be hidden behind a hemorrhage. Indeed, about 7% of ICHs are due to an underlying neoplasm (*2,3,6,35*). On the other hand, some hemorrhagic nonneoplastic lesions may mimic neoplastic lesions (*7–12*).

Five to 10% of all brain tumors develop hemorrhage of some type because of fast-growing and high vascularization with an irregular and fragile vascular architecture (*36*). Bleeding is the first clinical sign of neoplastic disease in 9%–58% of patients harboring hemorrhagic neoplasms (*1,34*). Hemorrhage is more common in metastatic tumors, followed by primary brain tumors. Metastatic lesions—including melanoma, bronchogenic carcinoma, choriocarcinoma, and hypernephroma—are known to carry a high risk of hemorrhage. Of the primary brain tumors, glioblastoma appears to be the most common source of ICH. Oligodendrogliomas also have a predilection for hemorrhage and do so more frequently than astrocytomas. Ependymomas and medulloblastomas also have been associated with ICH. Benign tumors rarely hemorrhage. In this group, pituitary adenomas and meningiomas are the lesions most likely to develop this complication (*1,34*).

Although CT and MRI can provide useful information, distinguishing with confidence hemorrhagic intracranial
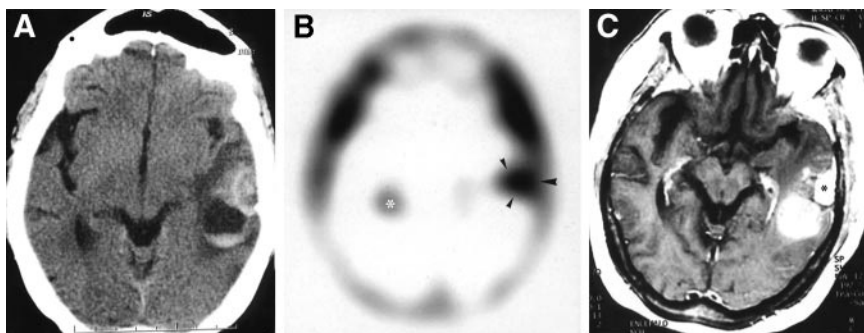
FIGURE 5. Patient 10: 63-y-old woman with sudden onset of aphasia and mild right hemiparesis. Medical history revealed arterial hypertension. (A) Emergency CT scan shows atypically located complex mass in left parietal region. Lesion is mainly hyperdense with round-shaped component presenting fluid–fluid level. (B) Early ^{99m}Tc-MIBI SPECT image shows focal area of high uptake (ER = 2.13) in area of lesion (arrowheads). Contralateral high-activity area is related to physiologic choroids plexus uptake (asterisk). (C) T1-weighted MR image after intravenous gadolinium administration shows strongly enhancing extracerebral lesion (asterisk) with meningeal tail sign. Diagnosis of meningioma was confirmed after surgical excision.

TABLE 1
Clinical Data and ^{99m}Tc-MIBI Uptake in 29 Patients with ICH

Patient no.	Age (y)	Sex	Location	Visual analysis (early images)	ER	DR	RI	Diagnosis
1	52	M	L occipital	Positive	3.95	1.5	0.38	Lung cancer metastasis
2	72	F	L frontal	Positive	2.13	1	0.46	Malignant cutaneous melanoma metastasis
3	60	F	L occipital	Positive	3.3	1.9	0.57	Hypernephroma metastasis
4	80	M	R frontal	Positive	3.12	3.19	1.02	Colon cancer metastasis
5	63	F	R frontal	Positive	2	1.6	0.8	Malignant cutaneous melanoma metastasis
6	50	M	R occipital	Positive	5.5	3.3	0.6	Lung cancer metastasis
7	63	M	R frontotemporal	Positive	2	2	1	Glioblastoma multiforme
8	52	M	R frontal	Positive	2.1	2	0.95	Glioblastoma multiforme
9	51	M	L parietal	Positive	3.4	2	0.6	Anaplastic ependymoma
10	63	F	L parietal	Positive	2.13	2.2	1.03	Angioblastic meningioma
11	28	F	Midbrain, R superior cerebral pedicle and R thalamus	Negative	1.05	1	0.95	Vascular degenerative disease
12	27	F	L parietal	Negative	1.08	0.98	0.9	Vascular degenerative disease
13	56	M	R temporoparietal	Negative	0.96	0.9	0.93	Vascular degenerative disease
14	40	M	R parietal	Negative	1.02	0.97	0.95	Vascular degenerative disease
15	63	F	L insular	Negative	0.97	0.98	1.01	Vascular degenerative disease
16	36	M	R thalamus	Negative	1	1.01	1.01	Vascular degenerative disease
17	50	F	L frontal	Negative	0.95	1.02	1.07	Vascular degenerative disease
18	47	F	L frontal	Negative	0.91	0.98	1.07	Vascular degenerative disease
19	38	M	R frontal	Negative	1.08	1.08	1	Vascular degenerative disease
20	60	M	L occipital	Negative	1	1.03	1.03	Vascular degenerative disease
21	76	F	L parietal	Negative	1.04	1	0.96	Vascular degenerative disease
22	78	M	R frontal	Negative	1.1	1	0.9	Vascular degenerative disease
23	72	F	L temporal	Negative	1.06	1.09	1.02	Vascular degenerative disease
24	51	M	R cerebellar hemisphere	Negative	1	1.06	1.06	Vascular degenerative disease
25	62	F	R occipital	Negative	1.12	1.03	0.92	Vascular degenerative disease
26	48	F	L parietal	Negative	1.2	1.18	0.98	Sinus rectus thrombosis
27	52	F	R insular	Negative	1.3	1	0.77	Thrombosed middle cerebral artery giant aneurysm
28	58	M	R occipital, paratrigonal	Negative	0.89	0.92	1.03	Cavernous angioma
29	42	F	L temporal	Negative	0.9	0.95	1.05	Cavernous angioma

FIGURE 6. Graph shows ER values in 29 patients with intracerebral hemorrhagic brain lesions. Wide cutoff ranging between 1.3 and 2 is appreciable.

neoplasms from nonneoplastic hematomas is often difficult because of considerable overlap between the imaging findings of these 2 types of lesions (13–16). The high density of blood on CT and the varied appearance of hemoglobin products on MRI may obscure the presence of an underlying neoplasm (18). In addition, lesion enhancement may be indistinguishable from contiguous hemorrhagic areas of intrinsically high density or increased signal intensity (17,19). Moreover, on neuroradiologic imaging, the diagnosis of neoplasm-related hemorrhage is frequently based on evolution patterns, being delayed hematoma evolution, persistent edema, and diminished, irregular, or absent hemosiderin deposition signs of neoplastic ICH (13–15). Thus, a complex diagnostic protocol is frequently needed and a significantly delayed diagnosis can occur.

^{18}F-FDG PET and ^{11}C-methionine PET have been tested as diagnostic tools for the differential diagnosis of ICH. Because occasional spots of increased uptake of ^{18}F-FDG can be present around some hematomas and high uptake of ^{11}C-methionine can be observed at the periphery of both neoplastic and nonneoplastic hematomas, Dethy et al. (21) concluded that PET studies with these tracers were not helpful in distinguishing neoplastic and nonneoplastic intra-

cerebral hemorrhage. More recently, Ogawa et al. (16) examined 8 patients with neoplastic and nonneoplastic intracerebral hematomas. They observed that subacute nonneoplastic hematomas showed ^{11}C-methionine accumulation largely in accordance with contrast-enhanced areas on CT or MR images, whereas neoplastic hematomas showed increased ^{11}C-methionine accumulation that extended beyond the contrast-enhanced area on CT or MR images. They suggested that ^{11}C-methionine PET could distinguish neoplastic from nonneoplastic hematomas on the basis of differences in lesion extent compared with CT or MRI findings. Disadvantages of this method could be the high cost of the examinations and the poor availability of PET scanners.

^{99m}Tc-MIBI has been used as an imaging SPECT agent for various neoplasms, including brain tumors (23). MIBI is a lipophilic cation, whose retention seems to reflect primarily blood–brain barrier (BBB) damage (37); however, the cationic charge, lipophilic properties, and mitochondrial contents may play an important role in ^{99m}Tc-MIBI uptake, suggesting that the radionuclide may be distributed passively and taken up by metabolically active cells (38–40). Normal brain tissue shows minimal uptake of ^{99m}Tc-MIBI except for a great ^{99m}Tc-MIBI uptake in the choroid plexus.

The ^{99m}Tc-MIBI index obtained from early images (ER) is higher in more aggressive neoplasms. High-grade astrocytomas, glioblastoma multiforme, metastasis, intracranial meningiomas, and neurinomas show a high ^{99m}Tc-MIBI index. On the other hand, low-grade astrocytomas and nonneoplastic lesions show low or no ^{99m}Tc-MIBI accumulation (23–33).

We performed ^{99m}Tc-MIBI SPECT on patients suspected of harboring a neoplastic bleeding according to standard clinical and neuroradiologic criteria (32). Because there are no reports dealing with the ^{99m}Tc-MIBI SPECT findings of ICH, we performed a standard protocol that included both visual and semiquantitative analysis (23). ^{99m}Tc-MIBI SPECT showed no relevant uptake in all patients with nonneoplastic brain hemorrhage, whereas abnormally high uptake was revealed in the early images of all patients with tumor-related ICH. It can be speculated that in neoplastic hematomas the preexisting tumor BBB disruption allows ^{99m}Tc-MIBI accumulation in metabolically active neoplastic cells, whereas in nonneoplastic hematomas the absence of

FIGURE 7. Graph shows overall semiquantitative analysis results in our series. Statistically significant difference was found in ER ($P < 0.01$), DR ($P < 0.01$), and RI ($P < 0.05$) between neoplastic and nonneoplastic intracerebral hemorrhages.

metabolically active cells, in early phase, are responsible for the lack of ^{99m}Tc-MIBI accumulation independently by BBB integrity.

Although a statistically significant difference was found in the ER, DR, and RI between the 2 groups, the semiquantitative analysis was of no help in the discrimination of neoplastic ICHs because visible lesions on early images were neoplastic and invisible ones were nonneoplastic. Thus, we believe that visual analysis of SPECT images can be satisfactory in the evaluation of suspected neoplastic hemorrhagic lesions. Furthermore, because discriminating vascular degenerative disease from other etiologies in the nonneoplastic group is not possible on the basis of ^{99m}Tc-MIBI indices, it seems that delayed SPECT acquisition can be omitted when early images do not show areas of tracer uptake.

One limitation of this study could be the lack of ICH related to low-grade gliomas or inflammatory lesions, which represents a rare, but possible, event. According to the literature (23–25) and our own experience, dealing with about 100 cases (unpublished data), nonhemorrhagic low-grade gliomas and inflammatory lesions do not show ^{99m}Tc-MIBI uptake, but we are unable to predict how hemorrhage may influence the radiotracer uptake in such cases.

Further studies based on larger numbers of patients are needed to confirm our data.

CONCLUSION

Our data suggest that ^{99m}Tc-MIBI SPECT, together with neuroradiologic imaging, can play a role in the early non-invasive diagnostic work-up of hemorrhagic brain lesions, allowing a clear differentiation between neoplastic and non-neoplastic intraparenchymal hemorrhages. The high availability and low cost of this nuclear medicine technique can be considered additional advantages for the early diagnosis of neoplastic hemorrhages.

REFERENCES

1. Schrader B, Barth H, Lang EW, et al. Spontaneous intracranial haematomas caused by neoplasms. *Acta Neurochir (Wien)*. 2000;142:979–985.
2. Zuccarello M, Pardatscher K, Andrioli C, Fiore DL, Lavicoli R. Brain tumours presenting as spontaneous intracerebral haemorrhages. *Zentralbl Neurochir*. 1981; 42:1–8.
3. Iwama T, Ohkuma A, Miwa Y, et al. Brain tumours manifesting as intracranial haemorrhage. *Neurol Med Chir (Tokyo)*. 1992;32:130–135.
4. Jones NR, Blumbergs PC. Intracranial haemorrhages from meningiomas: a report of five cases. *Br J Neurosurg*. 1989;3:691–698.
5. Kim DG, Park CK, Paek SH, et al. Meningioma manifesting intracerebral haemorrhage: a possible mechanism of haemorrhage. *Acta Neurochir (Wien)*. 2000;142:165–168.
6. Kondziolka D, Bernstein M, Resch L, et al. Significance of haemorrhage into brain tumours: clinico-pathological study. *J Neurosurg*. 1987;67:852–857.
7. Bakshi R, Lindsay BD, Bates VE, Kinkel PR, Mechtler LL, Kinkel WR. Cerebral venous infarctions presenting as enhancing space-occupying lesions: MRI findings. *J Neuroimaging*. 1998;8:210–215.
8. Gokcil Z, Odabasi Z, Atilla S, Kutukcu Y, Vural O, Yardim M. Radiological follow-up in encapsulated intracerebral haematoma mimicking intratumoral bleeding. *Acta Neurol Belg*. 1998;98:27–31.
9. d'Avella D, Germanò A, Romano A, Cardia E, Tomasello F. Chronic encapsulated intracerebral hematoma: contribution of thallium-201 single photon emis-

sion computed tomography in preoperative diagnosis—case report. *Neurosurgery*. 1997;41:677–679.
10. Kuhner A, Scheidet D. Pseudotumour forms of spontaneous intracerebral haematomas. *Neurochirurgia*. 1988;31:118–122.
11. Schwartz A, Gass A, Hennerici M. Stroke vignette: epidural hematoma and hemorrhagic infarction mimicking a left temporal meningioma. *Cerebrovasc Dis*. 1999;9:251–252.
12. Preul MC, Villemure JG, Leblanc R, del Carpio-O'Donovan R. MRI diagnosis of brainstem cavernous angiomas presenting as tumours. *Can J Neurol Sci*. 1992; 19:376–382.
13. Atlas S, Grossman R, Gomori JM, et al. Hemorrhagic intracranial malignant neoplasm: spin-echo MR imaging. *Radiology*. 1987;164:71–77.
14. Destian S, Sze G, Krol G, Zimmerman RD, Deck MD. MR imaging of hemorrhagic intracranial neoplasm. *AJR*. 1989;152:137–144.
15. Destian S, Sze G, Krol G, Zimmerman RD, Deck MD. Magnetic resonance imaging of hemorrhagic neoplasm. *AJNR*. 1988;9:1115–1122.
16. Ogawa T, Hatazawa J, Inugami A, et al. Carbon-11-methionine PET evaluation of intracerebral hematoma: distinguishing neoplastic from non-neoplastic hematoma. *J Nucl Med*. 1995;36:2175–2179.
17. Gaul HP, Wallace CJ, Crawley AP. Reverse enhancement of hemorrhagic brain lesions on postcontrast MR: detection with digital image subtraction. *AJNR*. 1996;17:1675–1680.
18. Chan JH, Peh WC. Methemoglobin suppression in T2-weighted pulse sequences: an adjunctive technique in MR imaging of hemorrhagic tumors. *AJR*. 1999;173: 13–14.
19. Hanna SL, Langston JW, Gronemeyer SA. Value of subtraction images in the detection of hemorrhagic brain lesions on contrast-enhanced MR images. *AJNR*. 1991;12:681–685.
20. Sze G, Krol G, Olsen WL, et al. Hemorrhagic neoplasm: MR mimics of occult vascular malformations. *AJNR*. 1987;8:795–802.
21. Dethy S, Goldman S, Blecic S, Luxen A, Levivier M, Hildebrand J. Carbon-11-methionine and fluorine-18-FDG PET study in brain hematoma. *J Nucl Med*. 1994;35:1162–1166.
22. Parizel PM, Makkat S, Van Miert E, Van Goethem JW, van Den Hauwe L, De Schepper AM. Intracranial hemorrhage: principles of CT and MRI interpretation. *Eur Radiol*. 2001;11:1770–1783.
23. Baldari S, Restifo Pecorella G, Cosentino S, Minutoli F. Investigation of brain tumours with ^{99m}Tc-MIBI SPET. *Q J Nucl Med*. 2002;46:336–345.
24. Baillet G, Albuquerque L, Chen Q, Poisson M, Delattre JY. Evaluation of single-photon emission tomography imaging of supratentorial brain gliomas with technetium-99m sestamibi. *Eur J Nucl Med*. 1994;21:1061–1066.
25. Bagni P, Pinna L, Tamarozzi R, et al. SPET imaging of intracranial tumours with 99Tcm-sestamibi. *Nucl Med Commun*. 1995;16:258–264.
26. Maffioli L, Gasparini M, Chiti A, et al. Clinical role of technetium-99m sestamibi single-photon emission tomography in evaluating pretreated patients with brain tumours. *Eur J Nucl Med*. 1996;23:308–311.
27. Soler C, Beauchesne P, Maatougui K, et al. Technetium-99m sestamibi brain single-photon emission tomography for detection of recurrent gliomas after radiation therapy. *Eur J Nucl Med*. 1998;25:1649–1657.
28. De La Pena RC, Ketonen L, Villanueva-Meyer J. Imaging of brain tumors in AIDS patients by means of dual-isotope thallium-201 and technetium-99m sestamibi single-photon emission tomography. *Eur J Nucl Med*. 1998;25:1404–1411.
29. Naddaf SY, Akisik MF, Aziz M, et al. Comparison between ^{201}Tl-chloride and ^{99}Tc$^{(m)}$-sestamibi SPET brain imaging for differentiating intracranial lymphoma from non-malignant lesions in AIDS patients. *Nucl Med Commun*. 1998;19:47–53.
30. Nagamachi S, Jinnouchi S, Ohnishi T, et al. The usefulness of Tc-99m MIBI for evaluating brain tumors: comparative study with Tl-201 and relation with P-glycoprotein. *Clin Nucl Med*. 1999;24:765–772.
31. Del Sole A, Falini A, Ravasi L, et al. Anatomical and biochemical investigation of primary brain tumours. *Eur J Nucl Med*. 2001;28:1851–1872.
32. Nishiyama Y, Yamamoto Y, Fukunaga K, Satoh K, Kunishio K, Ohkawa M. Comparison of ^{99}Tc^m-MIBI with ^{201}Tl chloride SPET in patients with malignant brain tumors. *Nucl Med Commun*. 2001;22:631–639.
33. Connolly LP, Drubach LA, Ted Treves S. Applications of nuclear medicine in pediatric oncology. *Clin Nucl Med*. 2002;27:117–125.
34. Batjer HH, Kopitnik TA Jr, Friberg L. Spontaneous intracerebral and intracerebellar hemorrhage. In: Youmans J, ed. *Neurological Surgery*. IV ed. Philadelphia, PA: WB Saunders Co.; 1996:1449–1469.
35. Jellinger K. Pathology and aetiology of ICH. In: Pia HW, Langmaid C, Zierski J, eds. *Spontaneous Intracerebral Haematoma*. New York, NY: Springer; 1980: 13–29.

36. Nutt SH, Patchell RA. Intracranial hemorrhage associated with primary and secondary tumors. *Neurosurg Clin North Am.* 1992;3:591–599.

37. Staudenherz A, Fazeny B, Marosi C, et al. Does ^{99m}Tc-sestamibi in high grade malignant brain tumors reflect blood-brain barrier damage only? *Neuroimage.* 2000;12:109–111.

38. Chiu M, Kronauge JF, Piwnica-Worms D. Effect of mitochondrial and plasma membrane potentials on accumulation of hexakis (2-methoxyisobutylisonitrile) technetium(I) in cultured mouse fibroblasts. *J Nucl Med.* 1990;31:1646–1653.

39. Crane P, Laliberte R, Heminway S. Effect of mitochondrial viability and metabolism of technetium-99m-sestamibi. *Eur J Nucl Med.* 1993;20:20–25.

40. Savi A, Gerundini P, Zoli P, et al. Biodistribution of Tc-99m-methoxy-isobutyl-isonitrile (MIBI) in humans. *Eur J Nucl Med.* 1989;15:597–600.